Mass-resolved angular distribution of fission products in the ^{20}Ne + ^{232}Th reaction

R. Tripathi,[*] S. Sodaye, K. Sudarshan, and R. Guin

Radiochemistry Division, Bhabha Atomic Research Centre, Mumbai 400085, India

(Received 20 June 2013; revised manuscript received 10 July 2013; published 8 August 2013)

Mass-resolved angular distributions of fission product were measured in the ^{20}Ne + ^{232}Th reaction at $E_{\text{lab}} = 125.6$ and 142.5 MeV using the recoil catcher technique followed by offline γ-ray spectrometry. Angular anisotropy was found to decrease with increasing asymmetry of mass division. Angular anisotropies of the fission products in the symmetric region were significantly higher compared to those calculated using the statistical saddle-point model. Experimental anisotropies could be explained after considering the contribution from pre-equilibrium fission. Use of barrier energies corresponding to different mass asymmetry values in the calculations could reasonably reproduce the mass dependence of angular anisotropies. The role of barrier energies in governing the angular anisotropy indicates that the mass dependence of anisotropy may possibly be a distinguishing feature of pre-equilibrium fission from quasifission, in which the composite system escapes into the exit channel without being captured inside the saddle point.

I. INTRODUCTION

Fission fragment angular distribution has been one of the important probes for the investigation of the role of entrance-channel parameters in governing the fusion-fission dynamics. Depending on the entrance-channel parameters, namely, mass asymmetry, composite system mass, and beam energy, heavy-ion collision may be followed by compound nucleus fission (CNF) or non-compound nucleus fission (NCNF). In CNF, the composite system, formed after the capture of the projectile by the target nucleus, equilibrates in various degrees of freedom to form a fully equilibrated compound nucleus, which subsequently undergoes fission. In NCNF, the composite system undergoes fission without forming a fully equilibrated compound nucleus. The NCNF may further be divided into quasifission [1], fast fission [2,3], and pre-equilibrium fission [4]. In quasifission, the contact configuration is more elongated than the fission saddle point and the composite system undergoes fission without being captured inside the saddle point [1]. In the fast-fission process, there is no barrier in the exit channel to trap the composite system, and the composite system undergoes fission without forming a fully equilibrated compound nucleus. In the pre-equilibrium fission process [4], it is assumed that the composite system equilibrates in all degrees of freedom before fission, except K degree of freedom, K being the projection of the total angular momentum vector on the nuclear symmetry axis. Quasifission and pre-equilibrium fission processes are expected to be the dominant NCNF processes at beam energies not too high compared to the entrance-channel Coulomb barrier. According to the pre-equilibrium fission model of Ramamoorthy and Kapoor [4], pre-equilibrium fission is observed for reaction systems with entrance-channel mass asymmetry [$\alpha = |A_{\text{P}} - A_{\text{T}}|/(A_{\text{P}} + A_{\text{T}})$, where A_{P} and A_{T} are the projectile and target mass numbers, respectively] less than the Businaro-Gallone critical-mass asymmetry (α_{BG}) [5].

The angular distribution of fission fragments/products from CNF can be described by the statistical saddle-point model (SSPM) [6,7], according to which a spectrum of K states is populated at the saddle point which is characterized by a Gaussian distribution. Application of SSPM [6,7] is based on the assumptions that K is a good quantum number beyond the saddle point and fission fragments separate along the nuclear symmetry axis. Though the SSPM calculations described well the fission fragment/product angular distributions for CNF, deviations were observed for many reaction systems, indicating the contribution from NCNF [8–13]. In the actinide region, particularly for the heavier actinides, a significant contribution from quasifission and pre-equilibrium fission is expected due the compact saddle point and small fission barrier, respectively. Hinde *et al.* [10,11] observed strong deviation of the fission fragment angular distribution in ^{16}O + ^{238}U reaction at near- and sub-barrier energies from SSPM calculations. Hinde *et al.* [10,11] proposed an orientation-dependent quasifission model to explain the anomalously large angular anisotropies. According to this model, capture of the projectile predominantly takes place through the collision with the tip of the deformed target nucleus at near- and sub-barrier energies. In the case of tip collision, the contact configuration would be outside the saddle point and, therefore, the composite system may undergo quasifission. However, Nishio *et al.* [14] reported that the evaporation residue cross sections for ^{16}O + ^{238}U reaction are in agreement with the statistical theory calculations. In these studies, it was proposed that the anomalous fission fragment angular distribution in this reaction may be due the pre-equilibrium fission as $\alpha < \alpha_{\text{BG}}$ for this system. In the studies by Lestone *et al.* [15] and Nayak *et al.* [16], it was shown that the deviation from SSPM is pronounced for spin-zero projectile-target systems at near- and sub-barrier energies as the fissioning system retains a memory of the entrance-channel K distribution in the case of pre-equilibrium fission. In the studies by Thomas *et al.* [17], it was shown that the angular distribution may be anomalous even for the reactions with $\alpha > \alpha_{\text{BG}}$ at near- and sub-barrier energies as the Businaro-Gallone critical-mass asymmetry (α_{BG}) shifts

_____
[*]rahult@barc.gov.in

towards a higher value when fusion is initiated at a larger distance at sub-barrier energies. In these studies a time-dependent variance of K distribution was used in the calculation of angular anisotropy. After including the contribution from pre-equilibrium fission and coupling effects in the fusion process, angular anisotropy for several fissioning systems in the actinide region were explained [15–17]. John *et al.* [18] studied mass-resolved angular distribution of fission products in ^{11}B-, ^{12}C-, and ^{16}O-induced reactions on ^{232}Th. In this study a mass dependence of angular anisotropy (increase in angular anisotropy with decreasing mass asymmetry) was observed in the ^{16}O $+$ ^{232}Th reaction, which was attributed to the preference for symmetric fission for collision trajectories with large angular momentum. Later, Vorkapic and Invanisevic [19] explained this observation based on the contribution from pre-equilibrium fission. According to their model, the barrier energy and, thus, the fission time scale decrease as we move towards symmetry. Due to the change in the fission time scale, the contribution from pre-equilibrium fission as well as the variance of K distribution changes with mass asymmetry. The angular anisotropy is highest for symmetric fission as fission time scale is minimum and it decreases with increasing mass asymmetry.

Fission fragment/product angular distributions in reactions with low $Z_P Z_T$, particularly the mass dependence of angular anisotropy, have not been explored much. Such studies are important to understand the contribution from various NCNF processes in the actinide region. Mass dependence of angular anisotropy can give information whether quasifission or pre-equilibrium fission dominates in a given reaction. In the case of quasifission a mass dependence of anisotropy, if present, is expected to be opposite to that for pre-equilibrium fission as quasifission is expected to dominate the asymmetric mass region [20–24]. In the present work, mass-resolved angular distribution has been measured in the ^{20}Ne $+$ ^{232}Th reaction at $E_{\text{lab}} = 125.6$ and 142.5 MeV, which correspond to $E_{\text{c.m.}}/V_b$ values of 1.14 and 1.29, respectively. A large contribution from pre-equilibrium fission is expected at these beam energies. The results from the present measurements have been compared with those calculated using SSPM for CNF as well as with those obtained after considering the contribution from pre-equilibrium fission.

II. EXPERIMENTAL DETAILS

Experiments were carried out at Variable Energy Cyclotron Centre, Kolkata. Self-supporting targets of ^{232}Th were irradiated with ^{20}Ne beam with incident energy of 145 MeV for the measurement of fission-product angular distributions. Targets were mounted at $62.5°$ with respect to the beam direction. In one irradiation, target thickness was 2.28 mg/cm^2 so that the average energy at the center of the target was 142.5 MeV. In the other irradiation, a ^{232}Th target of thickness 3.38 mg/cm^2 was backed by 12.5 μm superpure aluminum catcher foil so that the average energy at the center of the target was 125.6 MeV. The energy degradation in the aluminum foil and target was calculated using the code TRIM [25]. Irradiations were carried

TABLE I. Nuclear data of the various fission products used in the present study [26].

Isotope	Half life ($T_{1/2}$)	E_γ (keV)	Abundance (%)
^{87}Kr	76.3 min	402.6	49.6
^{90}Y	3.19 h	202.5	97.3
^{91}Sr	9.63 h	749.8	23.6
^{92}Sr	2.71 h	1383.9	90.0
^{95}Zr	64.02 d	756.7	54.5
^{97}Zr	16.91 h	743.4	92.6
^{98}Nb	51.3 min	787.4	93.0
^{99}Mo	65.94 h	140.5	90.7
^{103}Ru	39.25 d	497.1	89.5
^{105}Ru	4.44 h	724.2	46.7
^{111}Pd^m	5.5 h	172.2	33.5
^{112}Pd	21.05 h	617.4	50
^{115}Cd^g	2.23 d	527.9	27.5
^{117}Cd^m	3.36 h	552.9	125
^{117}Sn^m	13.61 d	158.6	86.4
^{120}Sb^m	5.76 d	1023.3	99
^{122}Sb^g	2.70 d	564	70.8
^{124}Sb^g	60.2 d	602.7	98.4
^{126}Sb^g	12.46 d	414.8	83.2
^{126}I	13.02 d	388.6	32.2
^{127}Sb	3.85 d	685.7	36.6
^{127}Xe^g	36.41 d	202.9	68.3
^{130}I^g	12.36 h	536.1	99.0
^{131}I	8.02 d	364.5	81.7
^{132}Te	3.204 d	228.2	88.1
^{133}I	20.8 h	529.9	87
^{141}Ce	32.5 d	145.4	48.2
^{143}Ce	33.04 h	293.27	42.8

out for about 45 h at both the beam energies. The fission products emitted in the forward hemi-sphere were stopped in the superpure aluminum foil of thickness 6.75 mg/cm^2 mounted on the inner wall of a cylindrical chamber of length 130 mm and diameter 155 mm. In the θ_{lab} range from $90°$ to $30°$, the foils covered the azimuthal angular range $0°$–$180°$. In the θ_{lab} range from $30°$ to $0.3°$, the azimuthal coverage by the foil mounted on the front surface of the cylinder was $360°$. Subsequent to the irradiation, catcher foils were cut into ten strips, each covering, on average, $\sim9°$. The catcher foil strips corresponding to different θ_{lab} were assayed for the γ-ray activity of the fission products using a precalibrated HPGe detectors coupled to a PC-based 4K-MCA. Decay of fission products was followed for about 2 months. The unambiguous identification of the fission products was done based on their characteristic γ rays and half-lives. Nuclear data of fission products for the present study were taken from Ref. [26] and are given in Table I. The γ-ray spectra of fission products were analyzed using the spectrum analysis software PHAST [27] to obtain the peak areas under the characteristic γ-ray peaks of the fission products. After correcting the peak areas for the decay of the fission products after the irradiation and during counting, their activities at the end of the irradiation were obtained. The yield of a fission product in a given strip "i" (σ_i) was calculated from its "end of irradiation activity (A_i)" using the following

equation:

$$\sigma_i = \frac{A_i}{N\phi(1 - e^{-\lambda T_{\mathrm{irr}}})(a_\gamma/100)\varepsilon_\gamma},\qquad (1)$$

where N is the number of target atoms per unit area, ϕ is the number of beam particles incident per unit time, λ is the decay constant of fission product, T_{irr} is the duration of irradiation, a_γ is the γ-ray abundance, and ε_γ is the full energy detection efficiency at the measured γ-ray energy. The yields of fission products in different strips were corrected for the solid angle using the following equation to obtain the fission product angular distributions in lab frame of reference:

$$W(\theta_{\mathrm{lab}}) = \frac{\sigma}{\pi\,[\cos(\theta_{1\mathrm{lab}}) - \cos(\theta_{2\mathrm{lab}})]},\qquad (2)$$

where σ is the yield of the fission product in a given strip, $\theta_{1\mathrm{lab}}$ and $\theta_{2\mathrm{lab}}$ are the angles corresponding to the edges of the strip. In the analysis, the data of the catcher foil close to $90°$ was not used due to the shadowing from the target holder. Also, at the higher beam energy, the yields in the next two foils close to $90°$ were combined so that the first data point corresponds to the average angle of the two foils.

III. RESULTS AND DISCUSSION

The lab angular distributions of fission products were transformed into a center-of-mass (c.m.) frame of reference assuming full momentum transfer. The standard kinematic equations were used with kinetic energies calculated using the prescription of Rossner *et al.* [28]. It should be mentioned here that, as the target in the present reaction is a heavy target, there would be a contribution from transfer-induced fission (TF) involving partial linear momentum transfer [29,30]. Thus, for many fission products, there may be a significant contribution from TF depending on its mass and A/Z. It has been shown in the earlier studies [29,30] that the major contribution to TF comes from proton and α transfer channels. Mass distribution studies in the ^{20}Ne + ^{232}Th reaction [31] have shown that the products with $A/Z > \sim 2.47$ are predominantly formed in TF. Therefore, angular anisotropy data of fission products with $A/Z > 2.47$, though shown in the figures, have not been considered for comparison with the theoretical calculations. The c.m. angular distributions of fission products at $E_{\mathrm{lab}} = 125.6$ and 142.5 MeV are shown in Figs. 1 and 2, respectively. Angular distributions of fission products with $A/Z > 2.47$ are shown as open circles. There may be a contribution from TF
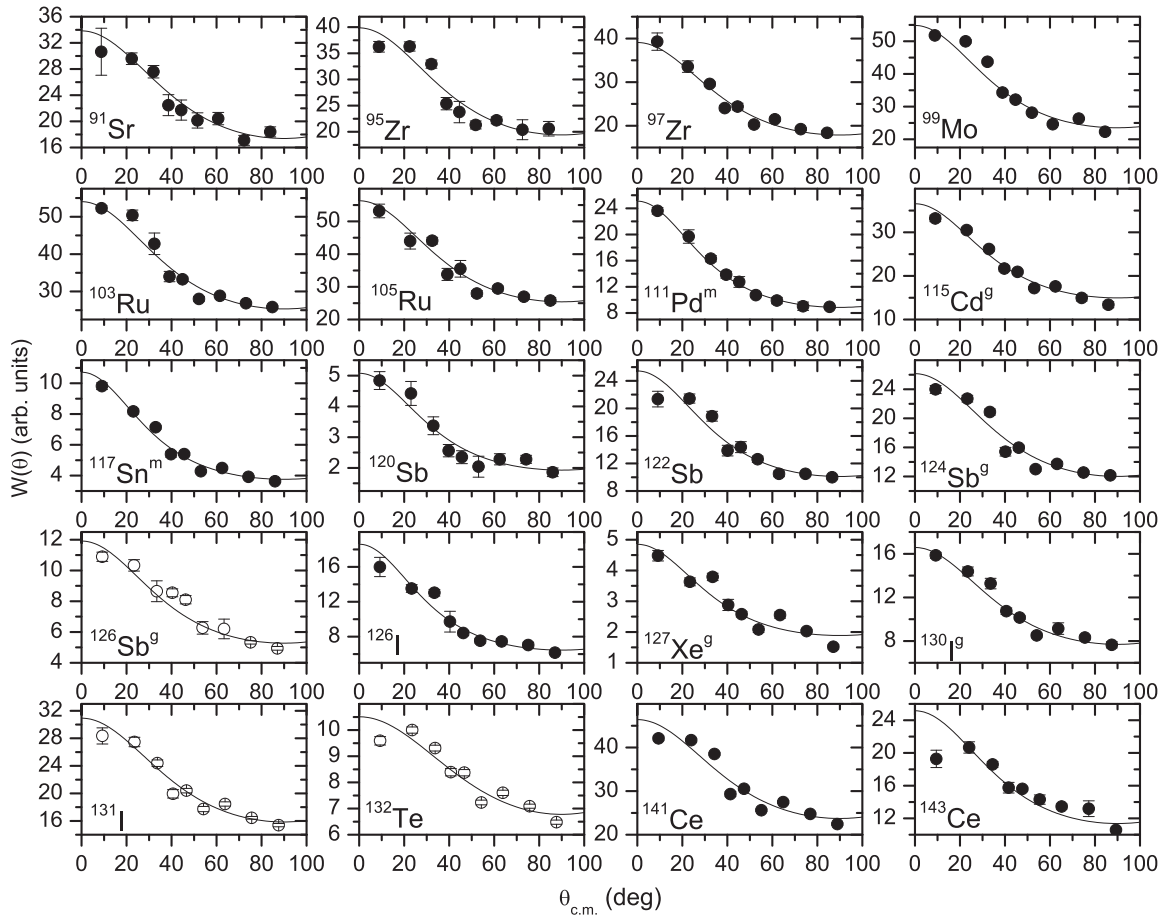

FIG. 1. Center-of-mass (c.m.) angular distributions of various fission products formed in the ^{20}Ne + ^{232}Th reaction at $E_{\mathrm{lab}} =$ 125.6 MeV. Solid black circles represent the experimental c.m. angular distribution of fission products predominantly formed in full momentum transfer fission ($A/Z \leqslant 2.47$). Open circles represent the experimental c.m. angular distributions of fission products predominantly formed in transfer-induced fission ($A/Z > 2.47$). Solid lines are fitted curves.
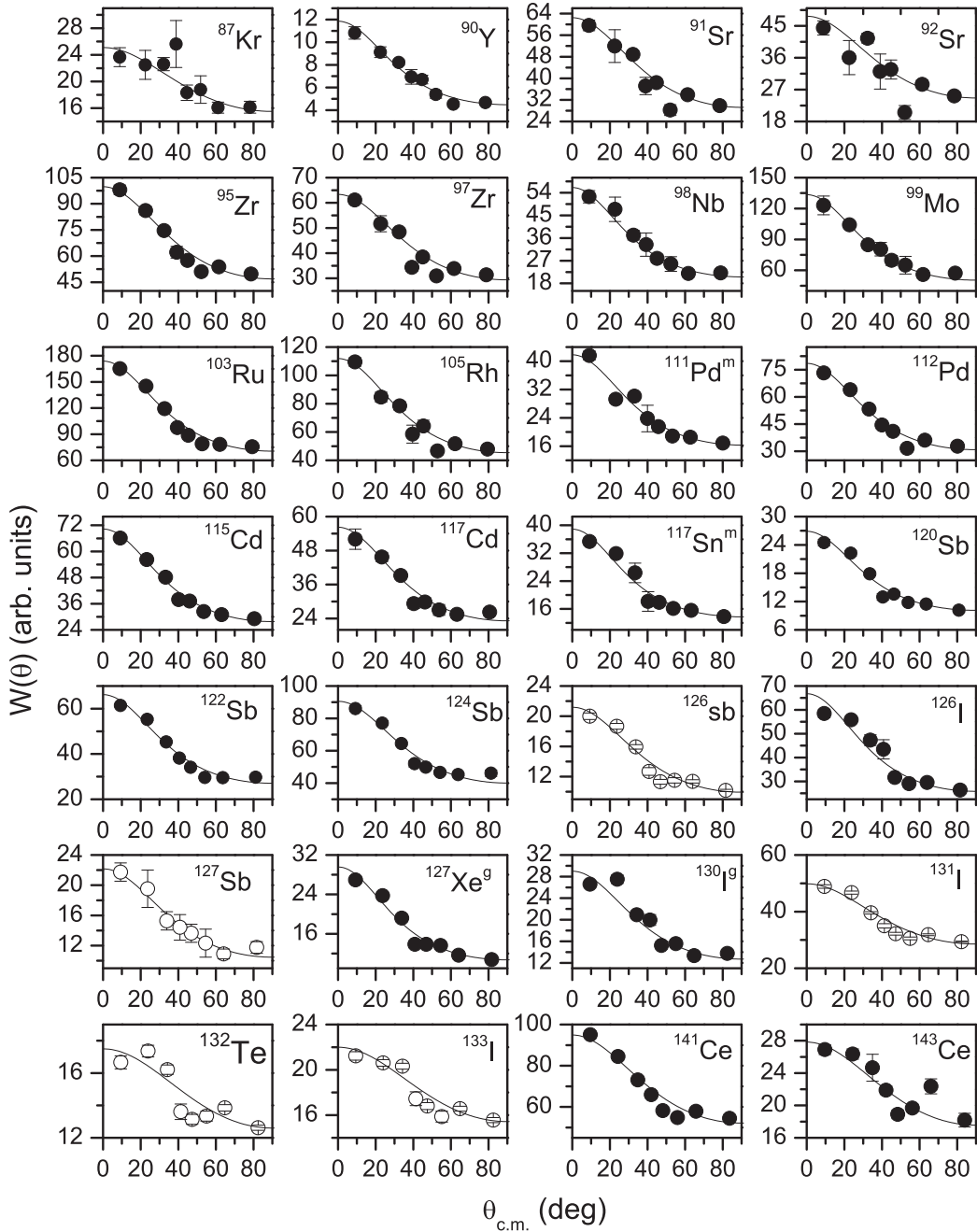
FIG. 2. Same as Fig. 1, for $E_{\text{lab}} = 142.5$ MeV.

to fission products even with lower A/Z due to the decay of the comparatively more neutron-rich precursor. However, as beam energies of the present studies are significantly higher than the entrance-channel Coulomb barrier, contribution from TF relative to full momentum transfer fission is expected to be small. Thus, as an approximation, fission products with $A/Z < 2.47$ have been assumed to be formed in full momentum transfer events. As was done in the earlier studies [13,32,33], the c.m. angular distributions were fitted using statistical theory expression

$$W(\theta_{\text{c.m.}}) = C \sum_{l=0}^{\infty} \frac{(2l+1)^2 T_l e^{-\frac{(l+1/2)^2 \sin^2 \theta_{\text{c.m.}}}{4K_0^2}} J_0\left[i(l+1/2)^2 \sin^2 \theta_{\text{c.m.}}/4K_0^2\right]}{\left(2K_0^2\right)^{1/2} \text{erf}\left[(l+1/2)/\left(2K_0^2\right)^{1/2}\right]}, \qquad (3)$$
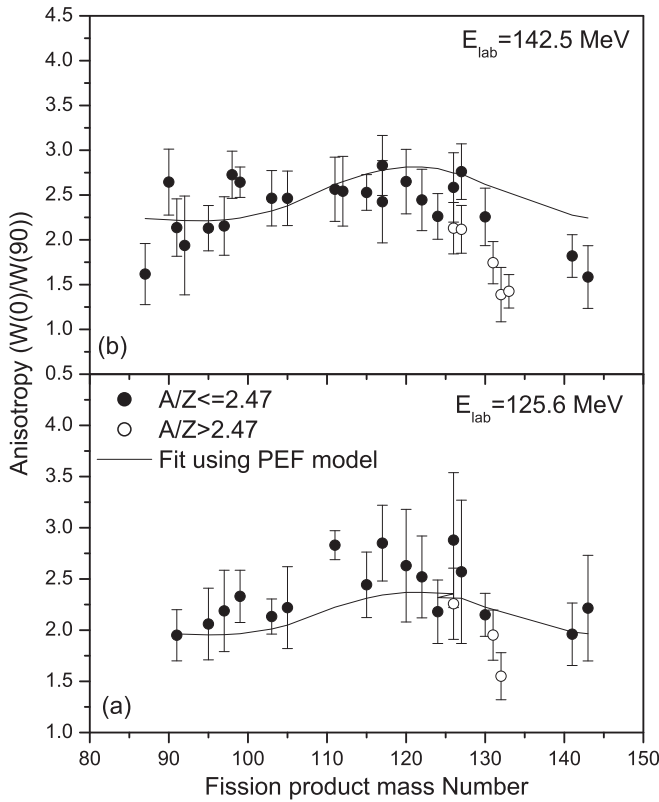
FIG. 3. (a) Angular anisotropies of various fission products formed in the ^{20}Ne + ^{232}Th reaction at $E_{\text{lab}} = 125.6$ MeV. Solid and open circles carry the same meaning as in Figs. 1 and 2. (b) Same as (a), but for $E_{\text{lab}} = 142.5$ MeV. Solid lines are fit to experimental anisotropies using pre-equilibrium fission model.

with K_0^2 and C as free parameters. T_l is the transmission coefficient, J_0 is the zeroth-order Bessel function, and "erf" is the error function. Fitted curves are shown as solid lines in Figs 1 and 2. Angular anisotropies obtained by fitting the c.m. angular distributions at $E_{\text{lab}} = 125.6$ and 142 MeV are shown in Figs. 3(a) and 3(b), respectively, as a function of fission product mass. Angular anisotropies for the fission products with $A/Z > 2.47$ are also shown as open circles in these figures. The uncertainties on the angular anisotropy values are due to the fitting error. A clear dependence of the angular anisotropies on the fission product mass can be seen from these figures. As observed in the ^{16}O + ^{232}Th reaction [18], angular anisotropy is highest in the symmetric region, which corresponds to the fission product mass of about ~121, after considering the emission of about ~10 neutrons during the fission process, as calculated using the prescription of Kozuline et al. [34]. As seen from Fig. 3, angular anisotropy decreases with increasing mass asymmetry. This trend is opposite to that observed in proton- and α-induced fission of ^{232}Th [35–39]. As beam energies of the present study are higher than the entrance-channel Coulomb barrier and $Z_P Z_T$ (=900) for the present system is small, contribution from quasifission is not expected to be significant. Even in the case of contribution from quasifission, a larger anomaly is expected in the asymmetric mass region which is dominated by quasifission [20–24].

In the study of fission fragment angular distribution in the ^{48}Ca + ^{168}Er reaction by Trotta et al. [24], it was observed that the angular distribution of asymmetric fission fragments have a forward-backward asymmetry due to the quasifission. Thus, the larger anisotropy of symmetric fission products observed in the present study cannot be attributed to quasifission. As suggested by Vorkapic and Ivansevic [19], this trend can be attributed to the contribution from pre-equilibrium fission. For the present system, $\alpha < \alpha_{\text{BG}}$; therefore, a large contribution from pre-equilibrium fission is expected as the fissioning system is characterized by a small fission barrier and high temperature [4]. Due to the variation in barrier energies with asymmetry of mass division, and, in turn, of the fission time scale, variance of K distribution as well as the contribution from pre-equilibrium fission changes with asymmetry of mass division. For the CNF, angular anisotropy was calculated using the statistical theory equation (3) with K_0^2 given by the equation

$$K_0^2 = \frac{I_{\text{eff}} T}{\hbar^2},\tag{4}$$

where I_{eff} is the effective moment of inertia of the fissioning nucleus at the saddle point and is given by the equation

$$\frac{1}{I_{\text{eff}}} = \frac{1}{I_{\|}} - \frac{1}{I_{\perp}},\tag{5}$$

where $I_{\|}$ and $I_{\perp}$ are, respectively, the moments of inertia values for rotation about the nuclear symmetry axis and an axis perpendicular to nuclear symmetry axis. The temperature T at the saddle point was calculated using the equation

$$T = \sqrt{(E^* - B_f - E_{\text{rot}} - E_\nu)/(A_f/8)},\tag{6}$$

where E^* ($=E_{\text{c.m.}} + Q_{gg}$) is the excitation energy of the compound nucleus, $E_{\text{c.m.}}$ is the projectile energy in the c.m. frame of reference, and Q_{gg} is the ground-state Q value for the formation of the compound nucleus. B_f is the l-dependent fission barrier for symmetric fission, E_{rot} is the rotational energy of the fissioning nucleus at the saddle point and was approximated as $l^2 \hbar^2 / 2 I_{\perp}$, and E_ν is energy lost in the emission of prefission neutrons. To calculate E_ν, the number of prefission neutrons was calculated using the prescription of Kozuline et al. [34]. The level density was taken as $A_f/8$ MeV^{-1}, where A_f is the mass of the fissioning nucleus. In the present calculations, fissioning nucleus mass was approximated as that of the compound nucleus, as the majority of the neutrons are emitted after the fission. The quantities B_f, $I_{\|}$, $I_{\perp}$ for different l waves were calculated for symmetric fission using the model of Sierk [40], based on the liquid drop potential energy. The compound nucleus l distribution, calculated using the code CCFUS [41], was approximated as the l distribution of the fissioning nucleus. This is a valid approximation as almost the entire fusion cross section goes to fission. As beam energies are significantly above the entrance-channel barrier, coupling effects were not considered in the CCFUS [41] calculations. Angular anisotropies, calculated using SSPM, are given in Table II. For comparison, mass-averaged experimental anisotropies are also given in this table. To calculate average angular anisotropies, mass yields were taken from Ref. [31]. As seen from this

TABLE II. Comparison of mass averaged experimental anisotropies with those calculated using statistical saddle-point model (SSPM) [6,7]. To calculate mass averaged anisotropies, mass yields were taken from Ref. [31].

E_{lab} (MeV)	$\left\langle \frac{W(0)}{W(90)} \right\rangle_{\text{SSPM}}$	$\left\langle \frac{W(0)}{W(90)} \right\rangle_{\text{Experimental}}$
125.6	1.86	2.41 ± 0.11
142.5	2.07	2.43 ± 0.07

table, experimental anisotropies are higher than the SSPM calculations at both beam energies. The observed deviation can be attributed to the contribution from pre-equilibrium fission as $\alpha < \alpha_{\text{BG}}$ for the present reaction system. As fission barrier is close to the temperature of the fissioning nucleus at the saddle point, and even lower for high l waves, a large contribution from pre-equilibrium fission is expected for the present system. It can also be seen from Table II that the difference between the SSPM calculations and experimental values decreases with increasing beam energy. Nearly similar values of average angular anisotropies at the two beam

energies indicate that the pre-equilibrium fission is dominant at both beam energies. As anisotropies calculated using SSPM increase with increasing beam energy due to the increase in the average angular momentum, the difference between the calculated and experimental anisotropies decreases with increasing beam energy.

To include the contribution from pre-equilibrium fission, calculations were performed using the model given in Refs. [16,17]. According to this model, the probability $[W(\theta_{\text{c.m.}})]$ of emission of fission fragments at an angle $\theta_{\text{c.m.}}$ is given as

$$W(\theta_{\text{c.m.}}) = W_{\text{CNF}}(\theta_{\text{c.m.}}) + W_{\text{PEF}}(\theta_{\text{c.m.}}), \qquad (7)$$

where subscripts CNF and PEF refer to the CNF and pre-equilibrium fission, respectively. As coupling effects in the fusion process have not been considered in view of the higher beam energies, Eq. (7) is simplified and does not contain the term for orientation dependence of the fusion probability. Also in the present calculations expression for fission fragment angular distribution was taken from Ref. [6]. Thus, $W_{\text{CNF}}(\theta)$ and $W_{\text{PEF}}(\theta)$ are given as (θ refers to $\theta_{\text{c.m.}}$ in the subsequent text)

$$W_{\text{CNF}}(\theta) = C \sum_{l=0}^{\infty} \frac{[1 - f_{\text{PEF}}(l)](2l+1)^2 T_l e^{-\frac{(l+1/2)^2 \sin^2 \theta}{4K_{0,\text{CNF}}^2}} J_0\left[i(l+1/2)^2 \sin^2 \theta / 4K_{0,\text{CNF}}^2\right]}{\left(2K_{0,\text{CNF}}^2\right)^{1/2} \text{erf}\left[(l+1/2)/\left(2K_{0,\text{CNF}}^2\right)^{1/2}\right]}, \qquad (8a)$$

$$W_{\text{PEF}}(\theta) = C \sum_{l=0}^{\infty} \frac{f_{\text{PEF}}(l)(2l+1)^2 T_l e^{-\frac{(l+1/2)^2 \sin^2 \theta}{4K_{\text{PEF}}^2}} J_0\left[i(l+1/2)^2 \sin^2 \theta / 4K_{\text{PEF}}^2\right]}{\left(2K_{\text{PEF}}^2\right)^{1/2} \text{erf}\left[(l+1/2)/\left(2K_{\text{PEF}}^2\right)^{1/2}\right]}, \qquad (8b)$$

where $f_{\text{PEF}}(l)$ is the pre-equilibrium fission probability given by the equation

$$f(l) = 1 - \exp\{-t_K / t_f(l)\}, \qquad (9)$$

where $t_{\text{f}}(l)$ is fission time scale and t_{K} is the time for K equilibration. The fission time scale $t_{\text{f}}(l)$ is given as

$$t_f(l) = \frac{2\pi}{\omega_{\text{eq}}} \exp\left(\frac{B_f(l)}{T}\right), \qquad (10)$$

where ω_{eq} is equal to 10^{21} s^{-1}. For pre-equilibrium fission, the time dependence of the variance of K distribution is given as $\sigma_K^2 = l^2 q^2 t_f T$, where q is a parameter representing the speed of K equilibration [15–17,42]. As discussed by Thomas *et al.* [17], the time for K equilibration $t_K \approx 4/q^2 T$, which corresponds to $\sigma_K = 2l$ representing a nearly flat K distribution.

The mass dependence of angular anisotropy comes from the dependence of the barrier energies on the mass asymmetry as suggested by Vorkapic and Ivanisevic [19]. Thus, the fission barrier in Eq. (10) is replaced with the barrier energies corresponding to different mass asymmetry values. The barrier energies based on the liquid drop model (LDM) were calculated using the procedure of Brack *et al.* [43]. According to this procedure, the shape of the fissioning nucleus is described

by three parameters, namely, elongation c, neck h, and mass asymmetry α. A plot of the potential energy surface of ^{252}Fm is shown in Fig. 4. In this plot, the mass asymmetry parameter α is replaced by the corresponding fission fragment mass. For the calculation of LDM potential energy of the fissioning nucleus, fission fragment masses were transformed into the corresponding value of the asymmetry parameter α using the equation given in Ref. [43]. The deformation energies shown in this plot are those obtained after minimizing the potential energy with respect to the neck parameter h except for small c values in the case of very asymmetric products, where it represents the upper limits. A fission valley in the symmetric mass region can be seen in the figure. The compound nucleus and typical symmetric and asymmetric shapes at the barrier corresponding to fission fragment masses of 126 and 96, respectively, are also shown in the figure. A plot of barrier energies as a function of fragment mass number is shown in Fig. 5. Fission fragment masses were transformed into the corresponding product masses by correcting for the neutrons (ν_{T}) evaporated during the fission process, as calculated using the prescription of Kozuline *et al.* [34]. As an approximation, the ν_{T} value was apportioned according to the mass ratio of the fragments. From the plot of Fig. 5, correction term for a given fission product with mass number A was obtained as
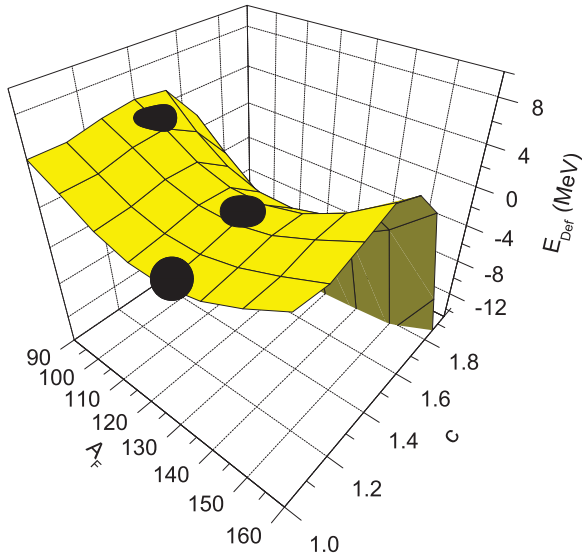
FIG. 4. (Color online) Liquid drop model potential energy surface of ^{252}Fm as a function of elongation parameter "c" and fission fragments mass number corresponding to different values of asymmetry parameter "α". The calculations were carried out using the procedure of Brack *et al.* [43]. Compound nucleus and typical shapes at the barrier for symmetric split (126 + 126) and asymmetric split (96 + 156) are also shown in the figure.

"$E_{\text{Def}}(A)$-$E_{\text{Def}}(A_{\text{Sym}})$," where $E_{\text{Def}}(A_{\text{Sym}})$ is the deformation or barrier energy for symmetric fission. The correction terms for different fission products were added to the fission barrier for symmetric fission [40] to account for the variation in barrier energy with asymmetry of mass division. This correction is based on the assumption that the l dependence of the barrier energy is independent of mass asymmetry. These barrier energies were used in Eq. (10) for the calculation of the fission time scale.
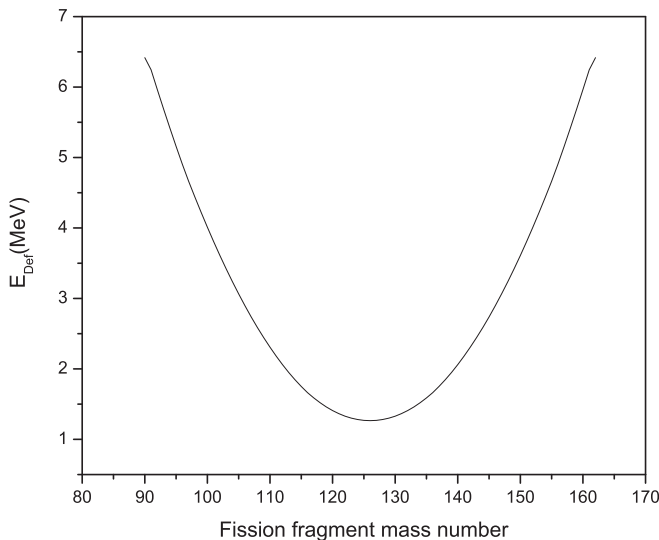

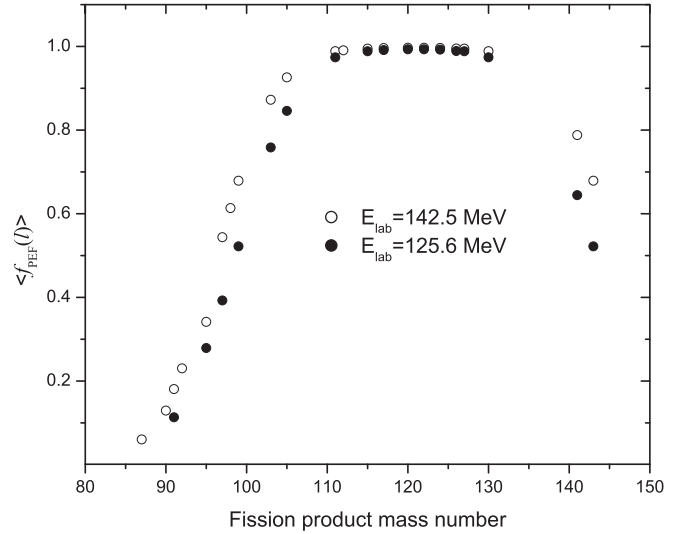FIG. 5. Plot of deformation or barrier energies (E_{Def}) as a function of fission fragment mass number.

FIG. 6. Plot of l-averaged pre-equilibrium fission probability ($\langle f_{\text{PEF}}(l) \rangle$) as a function of fission product mass number.

Angular anisotropies for CNF and PEF were calculated using Eqs. (8a) and (8b), respectively, with appropriate values of the variance of the K distribution, namely, $K_{0,\text{CNF}}^2$ and $K_{0,\text{PEF}}^2$. As discussed earlier, $K_{0,\text{CNF}}^2$ is given by Eq. (4), whereas, K distribution for pre-equilibrium fission is given by the equation

$$F_{\text{PEF}}(K) = \exp\left(\frac{K^2}{2K_{0,\text{CNF}}^2}\right) \times \exp\left(\frac{K^2}{2\sigma_K^2}\right) = \exp\left(\frac{K^2}{2K_{\text{PEF}}^2}\right),$$

$$(11)$$

with $\frac{1}{K_{\text{PEF}}^2} = \{\frac{1}{K_{0,\text{CNF}}^2} + \frac{1}{\sigma_K^2}\}$. In the calculation of angular anisotropies, the parameter q was kept as a free parameter, as was done in Refs. [16,17]. A combined fit (shown as solid lines in Fig. 3) to the data of both the beam energies gave q value as $(6.7 \pm 1.6) \times 10^9$ (MeV s)$^{-1/2}$. The q value obtained in the present study lies between the value of $\sim 5.4 \times 10^9$ (MeV s)$^{-1/2}$ and $\sim 8 \times 10^9$ (MeV s)$^{-1/2}$ obtained in Refs. [16,17], respectively. However, the extracted value of q should be considered approximate in view of the approximations involved in the calculations. The l-averaged pre-equilibrium fission probability ($\langle f_{\text{PEF}}(l) \rangle$) calculated using the q value of 6.7×10^9 (MeV s)$^{-1/2}$ is shown as a function of fission product mass number in Fig. 6. It can be seen from this figure that $\langle f_{\text{PEF}}(l) \rangle$ increases with decreasing mass asymmetry and approaches a nearly saturation value of unity in the symmetric region at both the beam energies. This is due to the decrease in the barrier energy with decreasing mass asymmetry, which is lowest for symmetric mass division. In the asymmetric mass region, $\langle f_{\text{PEF}}(l) \rangle$, values are systematically higher for higher beam energy than those at lower beam energies. This is mainly due to the population of additional l waves at higher beam energy for which $\langle f_{\text{PEF}}(l) \rangle$ is close to unity. In addition, comparatively higher temperature at $E_{\text{lab}} = 142.5$ MeV would also contribute to larger values of $\langle f_{\text{PEF}}(l) \rangle$.

Thus, present calculations explain reasonably the experimental anisotropies including their mass dependence after considering the contribution from pre-equilibrium fission. These studies show that the pre-equilibrium fission dominates in highly fissile system, and it has a dependence on the asymmetry of mass division. This observation suggests that the mass dependence of anisotropy may possibly be used as a distinguishing feature of pre-equilibrium fission from quasifission. More studies are required on the fission product/fragment angular distribution at near- and sub-barrier energies, particularly, in reaction systems with larger entrance-channel Coulomb repulsion where quasifission would dominate to confirm this conclusion.

IV. CONCLUSIONS

Measurement of mass-resolved angular distribution in the ^{20}Ne $+$ ^{232}Th reaction by the recoil catcher technique showed an increase in angular anisotropy with decreasing asymmetry of mass division in the fission process. This trend is opposite to that observed in proton- and α-particle-induced fission of ^{232}Th. For CNF, angular anisotropies were calculated using SSPM. At both beam energies, average experimental anisotropies were observed to be higher than the values calculated using SSPM. As $\alpha < \alpha_{\mathrm{BG}}$ for the present reaction system, the observed anomaly was attributed to the contribution from pre-equilibrium fission. Angular anisotropies were also calculated after including the contribution from pre-equilibrium fission. As suggested by Vorkapic and Ivanisevic [19], barrier energies corresponding to different mass asymmetry values were used in the calculations. The pre-equilibrium fission model calculations reasonably explained the experimental anisotropies including the mass dependence at both the beam energies. The results of the present measurements in the ^{20}Ne $+$ ^{232}Th reaction suggest that the mass dependence of anisotropy may be considered as a signature of the contribution from pre-equilibrium fission. Measurement of mass-resolved angular distribution at near- and sub-barrier energies will give more information on this aspect.

[1] W. J. Swiatecki, Phys. Scr. **24**, 113 (1981).

[2] C. Lebrun, F. Hanappe, J. F. Lecolley, F. Lefebvres, C. Ngo, J. Peter, and B. Tamain, Nucl. Phys. A **321**, 207 (1979).

[3] B. Borderie et al., Z. Phys. A **299**, 263 (1981).

[4] V. S. Ramamurthy and S. S. Kapoor, Phys. Rev. Lett. **54**, 178 (1985).

[5] U. L. Businaro and S. Gallone, Nuovo Cimento **5**, 315 (1957); K. T. R. Davies and A. J. Sierk, Phys. Rev. C **31**, 915 (1985).

[6] R. Vandenbosch and J. R. Huizenga, *Nuclear Fission* (Academic Press, London, 1973).

[7] I. Halpern and V. M. Strutinsky, in *Proceedings of the Second United Nations International Conference on Peaceful Uses of Atomic Energy, Geneva, 1958*, edited by J. H. Martens et al. (United Nations, Switzerland, 1958), Vol. 15, p. 408.

[8] V. S. Ramamurthy et al., Phys. Rev. C **32**, 2182 (1985).

[9] V. S. Ramamurthy et al., Phys. Rev. Lett. **65**, 25 (1990).

[10] D. J. Hinde, M. Dasgupta, J. R. Leigh, J. P. Lestone, J. C. Mein, C. R. Morton, J. O. Newton, and H. Timmers, Phys. Rev. Lett. **74**, 1295 (1995).

[11] D. J. Hinde, M. Dasgupta, J. R. Leigh, J. C. Mein, C. R. Morton, J. O. Newton, and H. Timmers, Phys. Rev. C **53**, 1290 (1996).

[12] S. Kailas, Phys. Rep. **284**, 381 (1997).

[13] B. B. Back, R. R. Betts, J. E. Gindler, B. D. Wilkins, S. Saini, M. B. Tsang, C. K. Gelbke, W. G. Lynch, M. A. McMahan, and P. A. Baisden, Phys. Rev. C **32**, 195 (1985).

[14] K. Nishio, H. Ikezoe, Y. Nagame, M. Asai, K. Tsukada, S. Mitsuoka, K. Tsuruta, K. Satou, C. J. Lin, and T. Ohsawa, Phys. Rev. Lett. **93**, 162701 (2004).

[15] J. P. Lestone, A. A. Sonzogni, M. P. Kelley, and R. Vandenbosch, Phys. Rev. C **56**, R2907 (1997).

[16] B. K. Nayak, R. G. Thomas, R. K. Choudhury, A. Saxena, P. K. Sahu, S. S. Kapoor, Raghav Verma, and D. Umarkanth, Phys. Rev. C **62**, 031601(R) (2000).

[17] R. G. Thomas, R. K. Choudhury, A. K. Mohanty, A. Saxena, and S. S. Kapoor, Phys. Rev. C **67**, 041601(R) (2003).

[18] Bency John et al., Phys. Rev. C **51**, 165 (1995).

[19] D. Vorkapić and B. Ivanišević, Phys. Rev. C **55**, 2711 (1997).

[20] K. Nishio, H. Ikezoe, S. Mitsuoka, I. Nishinaka, Y. Nagame, Y. Watanabe, T. Ohtsuki, K. Hirose, and S. Hoffmann, Phys. Rev. C **77**, 064607 (2008).

[21] K. Nishio, H. Ikezoe, I. Nishinaka, S. Mitsuoka, T. Ohtsuki, Y. Watanabe, Y. Aritomo, and S. Hofmann, Phys. Rev. C **82**, 044604 (2010).

[22] M. G. Itkis, I. M. Itkis, G. N. Knyazheva, and E. M. Kozuline, Nucl. Phys. A **834**, 374c (2010).

[23] A. Yu. Chizhov, M. G. Itkis, I. M. Itkis, G. N. Kniajeva, E. M. Kozuline, N. A. Kondratiev, I. V. Pokrovsky, R. N. Sagaidak, V. M. Voskressensky, and A. V. Yeremin, Phys. Rev. C **67**, 011603(R) (2003).

[24] Trotta et al., Prog. Theor. Phys. Suppl. No. **154**, 37 (2004).

[25] J. P. Biersack and J. F. Ziegler, TRIM 95.06, 1995.

[26] R. B. Firestone and V. S. Shirley, *Table of Isotopes*, 8th ed. (Wiley-Interscience, New York, 1999); U. Reus and W. Westmeier, At. Data Nucl. Data Tables **29**, 1 (1983).

[27] P. K. Mukhopadhyaya, in *Proceedings of DAE Symposium on Intelligent Nuclear Instrumentation (INIT-2001)*, edited by S. K. Kataria, P. P. Vaidya, P. V. Narurkar, and S. Roy (BARC, Mumbai, India, 2001), p. 307.

[28] H. H. Rossner, J. R. Huizenga, and W. U. Schröder, Phys. Rev. Lett. **53**, 38 (1984).

[29] G. K. Gubbi, A. Goswami, B. S. Tomar, B. John, A. Ramaswami, A. V. R. Reddy, P. P. Burte, and S. B. Manohar, Phys. Rev. C **59**, 3224 (1999).

[30] G. K. Gubbi, A. Goswami, B. S. Tomar, B. John, A. Ramaswami, A. V. R. Reddy, P. P. Burte, and S. B. Manohar, Phys. Rev. C **53**, 796 (1996).

[31] S. Sodaye, R. Tripathi, K. Sudarshan, and R.Guin, Phys. Rev. C **87**, 044610 (2013).

[32] R. Tripathi, K. Sudarshan, S. K. Sharma, K. Ramachandran, A. V. R. Reddy, P. K. Pujari, and A. Goswami, Phys. Rev. C **79**, 064607 (2009).

[33] Anomalous fission fragment angular distribution in the $^{11}B + {}^{243}Am$ reaction at near-barrier energies, R. Tripathi, K. Sudarshan, S. Sodaye, S. K. Sharma, and A. V. R. Reddy, Phys. Rev. C **75**, 024609 (2007).

[34] E. M. Kozuline, A. Ya. Rusanov, and G. N. Smirenkin, Phys. At. Nucl. **56**, 166 (1993).

[35] B. L. Cohen, B. L. Ferrel-Bryan, D. J. Coombe, and M. K. Hullings, Phys. Rev. **98**, 685 (1955).

[36] H. Kudo, Y. Nagame, H. Nakahara, K. Miyano, and I. Kohno, Phys. Rev. C **25**, 909 (1982).

[37] A. Goswami, S. B. Manohar, S. K. Das, A. V. R. Reddy, B. S. Tomar, and S. Prakash, Z. Phys. A **342**, 299 (1992).

[38] S. S. Kapoor, D. M. Nadkarni, R. Ramanna, and P. N. Rama Rao, Phys. Rev. **137**, B511 (1965).

[39] T. Datta, S. P. Dange, H. Naik, and S. B. Manohar, Phys. Rev. C **48**, 221 (1993).

[40] Arnold J. Sierk, Phys. Rev. C **33**, 2039 (1986).

[41] C. H. Dasso and S. Landowne, Comput. Phys. Commun. **46**, 187 (1987).

[42] T. Dossing and J. Randrup, Nucl. Phys. A **433**, 215 (1985).

[43] M. Brack, Jens Damgaard, A. S. Jensen, H. C. Pauli, V. M. Strutinsky, and C. Y. Wong, Rev. Mod. Phys. **44**, 320 (1972).